Scientific Reports Journal

OPEN ACCESS Freely available online

Research Article

Acupuncture at the Hegu (IC4) Point Detects Brain Oxygen Supply Disturbances in Patients with Brain Disorders: A fNIRS Study on Brain Oxygen Sensing

Wilhelm Ehleben[1], Jörn M. Horschig[2], Helmut Acker[1*]

[1]Forschungsinstitut für Notfallmedizin und Gesundheit (FONOG, UG), Kuntzestr. 59, D-44225 Dortmund, Germany

[2]Artinis Medical Systems, B.B. Einsteinweg 17, 6662 PW Elst, Netherlands

Correspondence to: Helmut Acker, Forschungsinstitut für Notfallmedizin und Gesundheit (FONOG, UG), Kuntzestr. 59, D-44225 Dortmund, Germany, E-mail: FNG.do@t-online.de

Received date: September 04, 2024; **Accepted date:** October 26, 2024; **Published date:** November 06, 2024

Citation: Ehleben W, Horschig JM, Acker H (2024) Acupuncture at the Hegu (IC4) Point Detects Brain Oxygen Supply Disturbances in Patients with Brain Disorders: A fNIRS Study on Brain Oxygen Sensing. Sci Rep J. 3:237.

ABSTRACT

The functional near-infrared spectroscopy (fNIRS) technique was introduced for general medical practice to measure brain blood oxygenation along with physiological parameters such as 4-channel EEG, heart rate, blood oxygenation, blood volume changes, and autonomic nerve activity. An artificial neuronal network was employed to adjust brain blood oxygenation measurements for changes in these physiological parameters. Early detection of cerebral blood flow disorders related to cognitive impairment, such as Alzheimer´s disease, appears to be feasible. Acupuncture with Hegu (LI4) was applied to stimulate brain neuronal networks in five control patients (CPs) and 5 brain disorder patients (BDPs). fNIRS recordings of brain Hb oxygenation indicated the efficacy of brain microcirculation and brain oxygen supply under central brain acupuncture stimulation in CPs. However, acupuncture stimulation of BDPs reveals deficits in brain microcirculation and oxygen supply. A single 20-second period of acupuncture stimulation results in brain hypoxia for BDPs but not for CPs, primarily due to the mismatch between arterial and venous microcirculation. fNIRS combined with subsequent artificial neural network analysis (ANN) of brain oxygen supply demonstrates potential as a highly effective and user-friendly method for recording early signs of brain microcirculation dysregulation and therapeutic progress.

Keywords: Acupuncture; Functional near-infrared spectroscopy; O_2Hb; HHb; Brain oxygen supply; Neurovascular coupling; Mitochondrial oxygen sensing; EEG Fourier power analysis; Brain disorder; Alzheimer´s disease; Artificial neural network

INTRODUCTION

The daily practice of general medicine is increasingly confronted with elderly people suffering from dementia related to Alzheimer´s disease, including post-stroke or traumatic brain disorders [1]. The early detection of mild cognitive impairment using fNIRS is crucial for initiating medical interventions [2]. In this study, we developed an application for measuring blood oxygenation status to identify cerebral blood flow disorders, as previously described [3]. Cerebral blood flow is influenced by physiological parameters such as heart rate (HR), blood volume changes (Pleth), hemoglobin oxygen saturation (SaO_2), autonomic nervous system activity (GSR), and neural cell activity (EEG) [4]. We measured these physiological parameters along with four bipolar EEG recordings (see Figure 1) simultaneously with fNIRS. Fourier power analysis yielded 23 parameters for analyzing the fNIRS signal with respect to cerebral and extracerebral oxygenation and deoxygenation factors (O_2Hb and HHb) [3]. The significance of each parameter for the fNIRS signal was evaluated using artificial neural network (ANN) analysis, which is recognized for nonlinear regression analysis of large medical datasets [5]. Additionally, O_2Hb-HHb relation plots were generated to analyze brain oxygen supply regulation.

We applied fNIRS to five healthy CPs and five BDPs, partly suffering from Alzheimer's disease, which is known to have disturbed neurovascular coupling (NVC) [5]. Various acupuncture points, including hé gǔ (Hegu, Union Valley, Large intestine meridian 4) [6], have demonstrated benefits in stroke rehabilitation by promoting neurogenesis and cell proliferation, regulating cerebral blood flow, preventing apoptosis, modulating neurochemicals, and improving impaired long-term potentiation and memory [7]. Based on our extensive acupuncture experience [8], we selected the Hegu point for a single 20-second acupuncture

session for each patient after obtaining written consent.

fNIRS with ANN analysis and O_2Hb-HHb relation plots revealed significant differences between CPs and BDPs owing to the varying impact of the 23 parameters on the kinetics of oxygenated and deoxygenated blood. The effect of Hegu acupuncture is comparable to the O_2Hb-HHb relationships observed under other NVC stimulations, such as touch, smell, taste, music, or calculations [3]. These types of studies need to be supplemented with more patients, utilizing O_2Hb-HHb relationships as early indicators of impaired NVC function in BDPs [5] or monitoring therapeutic success in the early treatment of cognitive deficiencies in general medical practice.

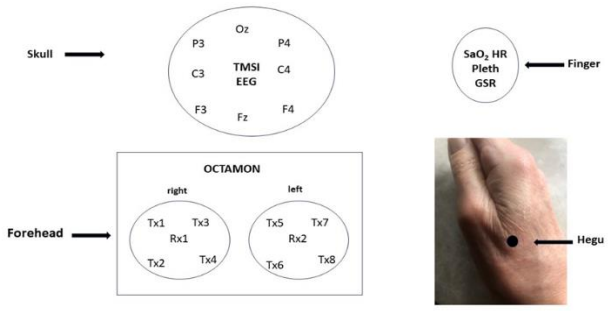

Figure 1: Depicts the experimental setup of the brain Octamon NIRS. The apparatus comprises Tx1–Tx8 diodes, which emit light at wavelengths of 751 and 843 nm. The emitted light traverses the brain tissue via reflection and is subsequently detected by the Rx1 and Rx2. This configuration enables the simultaneous measurement of oxygenated (O_2Hb) and deoxygenated (HHb) blood levels. Additionally, bipolar EEG signals (F3-F4, C3-C4, Fz-Oz, P3-P4), the GSR, the HR, and peripheral blood oxygen saturation (SaO_2) were monitored. Furthermore, blood volume changes are assessed utilizing photoplethysmography (Pleth) techniques.

MATERIALS AND EQUIPMENT

Figure 1 depicts a schematic representation of the head cap configuration, as previously described [3], which combines the 8-channel fNIRS OCTAMON device (manufactured by Artinis Medical Systems B. V, Elst, Netherlands) and a Bluetooth-enabled EEG TMSiMobi 6 channel amplifier (produced by TMSi, Oldenzaal, Netherlands). The fNIRS system utilizes multiple optodes (OCTAMON) primarily attached to the frontal region of the head. Eight transmitter diodes (Tx1-Tx4 on the right side and Tx5-Tx8 on the left side of the frontal head) emit light at wavelengths of approximately 751 nm and 843 nm to measure the kinetics of HHb and OHb, respectively, to assess NVC and cerebral blood flow autoregulation [8]. Near-infrared light within this wavelength range is predominantly absorbed by hemoglobin and to a lesser extent by water and lipids [9]. The emitted fNIRS light penetrates the brain tissue to a depth of 23 mm, with the deepest 5% reaching the gray cerebral tissue and 17.4% reaching a depth of 20.3 mm, indicating that a significant portion of the emitted light contains information about extracerebral regions such as the skin, bone, and muscles [10]. The fNIRS light was detected by two receivers, Rx1 and Rx2, after traversing the brain tissue, enabling the determination of O_2 Hb and HHb levels in the blood using a modified Lambert – Beer law. Additionally, four bipolar EEG signals (F3-F4, C3-C4, Fz-Oz, and P3-P4), the GSR for measuring autonomic nervous system activity (GSR), heart rate (HR), and arterial oxygen saturation (SaO_2) using photoplethysmography (Pleth), and blood volume changes in the fingertip were recorded at a rate of 256 Hz using the TMSiMobi system. The simultaneous measurement of various anatomical and physiological parameters during fNIRS registration, along with their identification in the fNIRS signal, is essential for obtaining a comprehensive understanding of NVC (Scholkmann et al., 2022). However, the interpretation of fNIRS signals in relation to the NVC under different neuronal stimulation conditions is restricted by anatomical and physiological interference [12]. The sampling rate of the fNIRS system was set at 50 Hz, but the data were upsampled to match the 256 Hz sampling rate of the other devices. The OxySoft program (Artinis Medical Systems B. V., Elst, Netherlands) was used for data recording, visualization, and computation. The collected data were stored in Excel files (Microsoft) for further analysis.

Patients

Ten patients who regularly sought consultation at a general medicine practice affiliated with FONOG (further information available at www.fonog.de) underwent a single brain oxygen supply assessment using functional near-infrared spectroscopy (fNIRS).Five patients (mean age 45±10 years) without brain disorders served as the control group (CPs), whereas five patients (mean age 62±22 years), including three with Alzheimer's disease (ICD10 G30.9, mean age 74±8 years), one who experienced a stroke episode (ICD10 I69.4, age 69 years), and one with autism (ICD10 F84.1, age 24 years), served as examples of brain disorder patients (BDPs). There were no statistically significant differences in age between the two groups ($p>0.05$). Patients provided written informed consent for the use of their data in this study using the Patient Consent Form Template (https://www.medizininformatik-initiative.de/). The institutional ethics committee of Ärztekammer Westfalen Lippe (Münster, Germany) was informed of the use of patient data for this study (2023-199-f-S).

EEG Time-Frequency Analysis

The EEG time series were processed as follows. First, detrending was performed by subtracting the least-squares fit of the straight line from the data. This was performed to remove any linear trends from the time series. Next, the time-frequency representation of the detrended data was obtained using short-time Fourier transform. A Hamming window of 128 points with 50% overlap was applied to the data during the transformation. This allowed for the analysis of temporal variations in the frequency content of the EEG signals. The amplitude values were converted to decibels (dB) to facilitate the visualization and analysis of the resulting spectrum. This conversion provides a logarithmic representation of the amplitude, which can better capture the dynamic range of EEG signals. To standardize the time-frequency representation, it was interpolated to a frequency of 256 Hz. This interpolation allowed for a uniform time-frequency resolution across the entire spectrum. Finally, the mean amplitudes for specific EEG bandwidths were computed. These bandwidths, commonly used in EEG analysis, include the delta (1-4 Hz), theta (4-8 Hz), alpha (8-13 Hz), beta (14-30 Hz), and gamma (30-100 Hz) bands. The mean amplitude values were calculated for bipolar EEG recordings, which involved the measurement of the electrical potential differences between two specific electrode placements. This provides information about the activity within specific brain regions or networks at different frequency ranges.

NVC Stimulation by Acupuncture

During the experimental session, participants were instructed to rest for a period of 10 min in a designated chair to acclimate to the fNIRS-EEG head cap. Subsequently, a single acupuncture treatment was administered according to a previously described method [13]. Specifically, single sterile steel needles measuring 0.22x13 mm (brand: Gushi-zhengzheng, Medical Device, Henang,

China) were utilized for the acupuncture procedure. Prior to needle insertion, acupuncture point Hegu, as depicted in Figure 1, was thoroughly disinfected. The needle was then superficially inserted into the skin, approximately 5 mm deep, by a medical doctor qualified as a consultant for acupuncture. Subsequently, the needle was gently rotated clockwise for 20 s until the rotation was impeded by tissue resistance.

Statistics

The data analysis began 10 s prior to the start of the 20-second acupuncture session. The fNIRS data were normalized, and the analysis was continued for approximately 30-40 seconds after the completion of acupuncture. A t-test was performed to compare the differences in recordings between the CPs (n=5) and BDPs groups (n=5). The impact of the 23 parameters on brain O_2Hb and HHb levels was assessed. The normal distribution of the data was controlled using a probability-probability (PP) test conducted in IBM SPSS Statistics version 27. The level of statistical significance was set at an alpha error level of $p<0.05$. Graphs were created using Microsoft Excel and PowerPoint.

The relative importance, comparable to the standardized beta coefficient of linear regression, of the 23 parameters for recalculating O_2Hb and HHb reactions to acupuncture NVC stimulation was assessed by ANN nonlinear regression (see Figure 6) composed of a 1-neural layer containing up to 18 units called the hidden layer (blue), one input layer containing the 23 explanatory parameters (left side), and one output layer containing the fNIRS measured oxygenation variables (right side, Multilayer Perceptron Network, IBM SPSS Statistics, Armonk, NY software version 27). Approximately 70% of the measured parameter values were used to train ANN. Subsequent testing by ANN used 30% of the measured parameter values. The time for training and testing was approximately 3 s, and the mean relative errors of recalculation were 0.057± 0.017 and 0.031 ± 0.01, respectively ($p<0.05$).

The English language and grammar were managed using the AJE Orcid Curie feature and Microsoft Addin Paperpal.

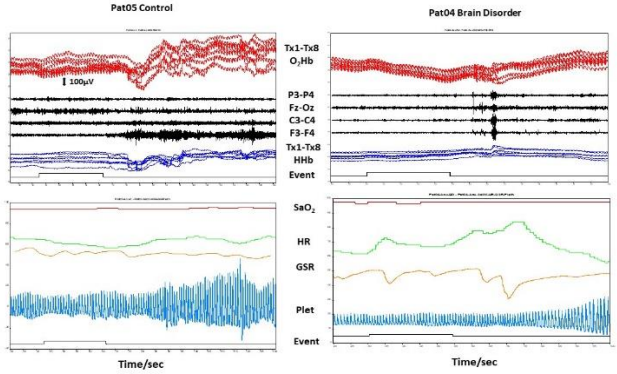

Figure 2: The left panel illustrates the O_2Hb and HHb responses to right-hand Hegu acupuncture (event) for 20 seconds in Pat05 CP. This was measured using frontal head fNIRS of Tx1-Tx8 O_2Hb (red) and HHb (blue), with concurrent registrations of bipolar EEGs (black, F3-F4, C3-C4, Fz-Oz, P3-P4). The lower panel displays the changes in SaO_2, HR, GSR, and Pleth during the same time period. The right panel of Figure 2 presents the O_2Hb and HHb responses to right-hand Hegu acupuncture (event) for 20 seconds in the Pat04 BD patient. This measurement was conducted using frontal head fNIRS of Tx1-Tx8 O_2Hb (red) and HHb (blue), with concurrent registrations of bipolar EEGs (black, F3-F4, C3-C4, Fz-Oz, P3-P4). The lower panel exhibits the simultaneous changes in SaO_2, HR, GSR, and Pleth during the same time period.

RESULTS

Figure 2 shows O_2Hb and HHb reactions to right-hand Hegu acupuncture (event) for 20 s on the left side of the Pat05 CP, as measured by frontal head fNIRS of Tx1-Tx8 O_2Hb (red) and HHb (blue), as well as simultaneous registrations of bipolar EEGs (F3-F4, C3-C4, Fz-Oz, P3-P4). The figure below shows the changes in SaO_2, HR, GSR, and Pleth during the same period. Data analysis generally began 10 s before the onset of NVC stimulation by acupuncture. O_2Hb started to increase and HHb decreased approximately 10 s after the acupuncture (event) was terminated. Concomitantly, the EEG activity increased significantly in F3-F4. The figure below shows some SaO_2 oscillations, while HR decreases a typical acupuncture reaction [13], probably due to a decrease in the GSR indicating sympathetic tone loss. Pleths show increasing blood volume changes, most likely superimposed with various frequency components attributed to respiration, sympathetic nervous system activity and thermoregulation [14]. Figure 2 shows O_2Hb and HHb reactions to riht-hand Hegu acupuncture (event) for 20 s on the right side of BD Pat04 as measured by frontal head fNIRS of Tx1-Tx8 O_2Hb (red) and HHb (blue) as well as simultaneous registrations of bipolar EEGs (F3-F4, C3-C4, Fz-Oz, P3-P4). O_2Hb decreased in response to acupuncture (event), and HHb increased correspondingly. Acupuncture was followed by enhanced EEG activity in all recordings. The figure below shows the simultaneous changes in SaO_2, HR, GSR, and Pleth during the same time period. While SaO_2 oscillates, HR finally decreases, and GSR shows corresponding sympathetic tone loss periods. The Pleth remained stable in the first phase and continued to increase with increasing blood volume.

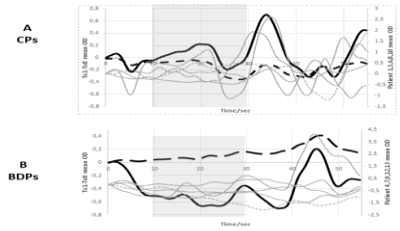

Figure 3: 3A presents the individual O_2Hb responses of channels T1-Tx8 of 5 CPs to acupuncture for 20 s (shaded area) as gray lines. The values of control patient 05 are represented by dotted gray lines. The mean O_2Hb response is depicted as a solid black bold line, whereas the mean HHb response is represented by a broken black bold line. Figure 3B displays the individual O_2Hb responses of channels T1-Tx8 of 5 BDPs to acupuncture for 20 s (shaded area) as gray lines. The values of BD patient 04 are represented by dotted gray lines. The mean O_2Hb response is depicted as a solid black bold line, whereas the mean HHb response is represented by a broken black bold line.

Figure 3A shows the single O_2Hb reactions of channels T1-Tx8 of five CPs to acupuncture for 20 s (shaded area) as gray lines. The values of CP 05 are shown by dotted gray lines. The mean O_2Hb reaction is shown by a solid black bold line, whereas the mean HHb reaction is shown by a broken black bold line. Figure 3B shows the single O_2Hb reactions of channels T1-Tx8 of five BDPs to acupuncture for 20 s (shaded area) as gray lines. The values of BDP 04 are indicated by dotted grey lines. The mean O_2Hb reaction is shown by a solid black bold line, whereas the mean HHb reaction is shown by a broken black bold line. The mean O_2Hb and HHb reactions of CPs and BDPs were significantly different ($p<0,05$), indicating an increase in the brain oxygen supply of CPs and an impairment in the oxygen supply of BDPs

under acupuncture at Hegu.

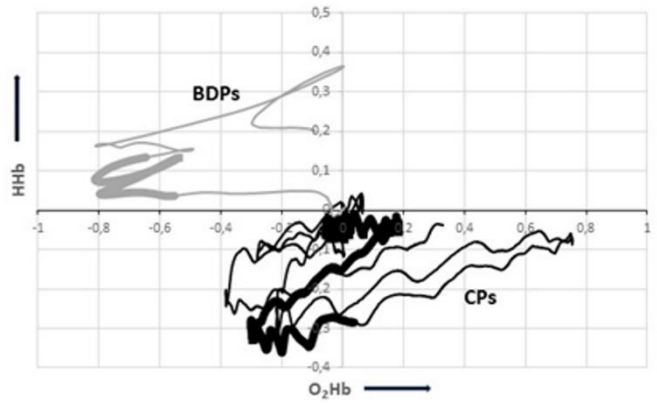

Figure 4: Illustrates the differences in brain oxygen supply in response to Hegu acupuncture between CPs and BDPs. The x-axis represents O_2Hb, and the y-axis represents the corresponding HHb optical density (OD) changes as the mean value of 5 CPs (black solid line) and 5 BDPs (gray solid line). The bold portion of the lines represents the 20 s period of acupuncture.

Figure 4 shows the differences in the brain oxygen supply in response to Hegu acupuncture between CPs and BDPs. The x-axis shows O_2Hb, and the y-axis shows the corresponding HHb optical density (OD) changes as the mean value of five CPs (black solid line) and five BDPs (gray solid line). The bold lines represent the time period of 20 seconds of acupuncture. CPs dominate with their meandering increasing O_2Hb and decreasing HHb values, indicating that microcirculation likely regulates the brain oxygen supply. BDPs contrast with nearly linear decreases in O_2Hb and increases in HHb, indicating microcirculation impairment during acupuncture-induced brain hypoxia. The question was whether this difference could be explained by the different importance of the 23 parameters measured and calculated for the fNIRS oxygenation recordings (Figure 2). Figure 5 illustrates this aspect.

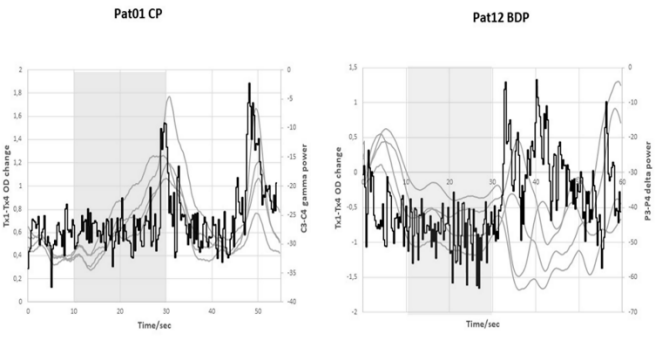

Figure 5: Demonstrates, on the left panel, the increasing Tx1-Tx8 O_2Hb response (gray lines) to acupuncture (shaded area) of 1 CP (Pat01) as well as the nearly parallel response of the gamma power of the EEG C3-C4 recording. On the right panel, gray lines indicate the decreasing Tx1-Tx8 O_2Hb response to acupuncture (shaded area) of 1 BDP (Pat12) as well as the nearly parallel response of the gamma power of the EEG P3-P4 recording.

Figure 5 shows on the left side the increasing Tx1-Tx8 O_2Hb reaction (gray lines) in response to acupuncture (shaded area) of 1 CP (Pat01), as well as the parallel reaction of the gamma power of the EEG C3-C4 recording. The right gray lines show the decreasing Tx1-Tx8 O_2Hb reaction in response to acupuncture (shaded area) at 1 BDP (Pat12) as well as the primary parallel reaction of the gamma power of the EEG P3-P4 recording. This visual assessment was replaced with an ANN for the first time [3].

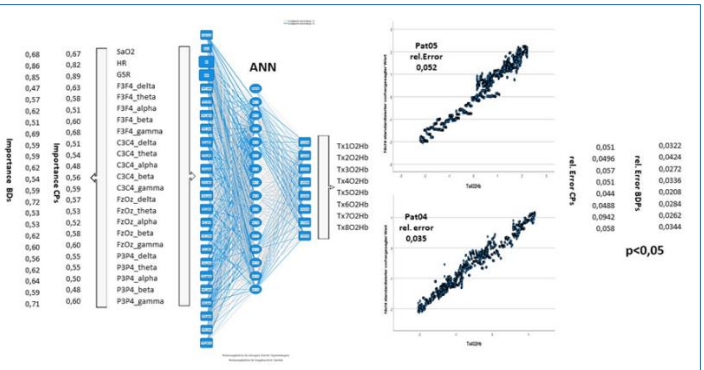

Figure 6: llustrates the Artificial Neural Network (ANN) configuration for analyzing the relative importance of 23 measured explanatory parameters (left side of the blue part) in estimating the Tx1-Tx8 O_2Hb- and HHb-dependent variables (right side of the blue part) under acupuncture, utilizing one hidden neural layer with 18 units (blue middle part). The left panel depicts the 23 explanatory parameters measured and calculated during the experiment and their relative importance used for recalculation. The thickness of the blue lines in the middle part between the 23 explanatory parameters and Tx1-Tx8 O_2Hb variables increases proportionally with increasing relative importance. The diagrams on the right side of the blue part demonstrate the linear relationship between the measured and ANN-recalculated Tx4 O_2Hb of 1 CP (Pat05) and Tx4 O_2Hb values for 1 BDP (Pat04) and the corresponding relative error. The relative error of calculation for the Tx1-Tx8 O_2Hb BDPs recordings was significantly lower than that for the Tx1-Tx8 O_2Hb CPs recordings.

Figure 6 shows the ANN setup for analyzing the relative importance of 23 measured explanatory parameters (left side of the blue part) for estimating the Tx1-Tx8 O_2Hb- and HHb-dependent variables (right side of the blue part) under acupuncture using one hidden neural layer with 18 units (blue middle part). The left panel shows the 23 explanatory parameters measured and calculated during the experiment, and their relative importance used for recalculation. The diagrams on the right side of the blue part show the linear relationship between the measured and ANN-recalculated Tx4 O_2Hb of 1 CP (Pat05) and Tx4 O_2Hb values for 1 BDP (Pat04), and the corresponding relative error. The relative error of the calculations for the BDP recordings was significantly lower than that of the CP recordings, suggesting a reduced and more linear influence of the 23 explanatory parameters.

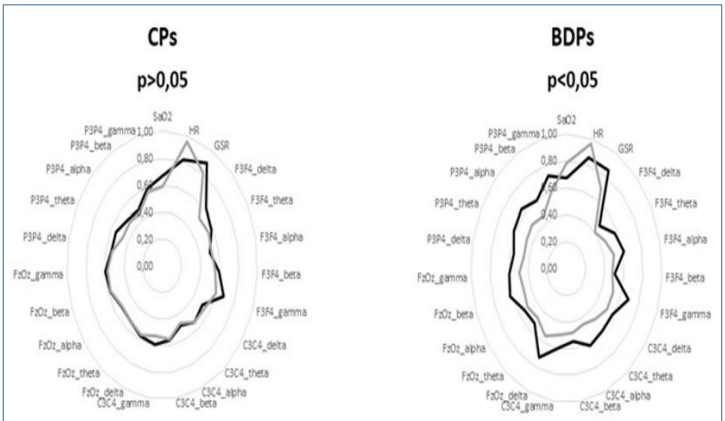

Figure 7: Presents a net diagram of the relative importance of 23 parameters for recalculating fNIRS O_2Hb (black line) and HHb changes (gray line) upon Hegu acupuncture for 20 s for 5 CPs (left side) and 5 BDPs (right side).

Figure 7 shows a net diagram of the relative importance of 23 parameters for recalculating fNIRS O_2Hb (black line) and HHb changes (gray line) upon Hegu acupuncture for 20 s for 5 CPs (left side) and 5 BDPs (right side). Peripheral factors, such as HR and GSR, are highly important for recalculating fNIRS O_2Hb changes in CPs and BDPs. Various brain power activities, as measured by EEG, are dominant in recalculating fNIRS O_2Hb changes in BDPs. Interestingly, net diagram analysis for BDPs revealed a significant difference between O_2Hb and HHb changes in contrast to those in CPs, indicating a mismatch of arterial and venous microcirculation control leading to brain hypoxia, as shown in Figures 2, 3, and 4.

DISCUSSION

Due to its relatively low spatial and temporal resolution and limited depth penetration of cortical tissue, NIRS exhibits significant limitations in determining whole-brain activity during complex cognitive or motor tasks. To address these constraints, NIRS can be integrated with the high temporal resolution of EEG to elucidate the metabolic and/or electrical activity of the brain, as described [3], facilitating investigations of slow hemodynamic changes related to rapid NVC dynamics [12]. Mean values derived from 20s fNIRS recordings may potentially compensate for the disparities in temporal and spatial resolution, yielding representative results of brain activities.

The direct stimulatory effect of acupuncture on central nervous system structures results in immediate changes in the limbic-paralimbic neocortical network, as measured by blood oxygenation level-dependent (BOLD) fMRI. These networks closely match the task-negative default mode network and the anticorrelated task-positive network as afferent targets [13]. Acupuncture can change the structural characteristics and functionality of synaptic plasticity by modulating synaptic proteins, inhibiting inflammatory responses in neural pathways, increasing mitochondrial energy metabolism, and decreasing amyloid beta deposition; for a review, see [15].

Regulation of cerebral blood flow (CBF) is essential for normal brain function. The mammalian brain has evolved a unique mechanism for CBF control known as NVC. This mechanism ensures a rapid increase in the rate of CBF and oxygen delivery to the activated brain structures. The NVC unit is composed of astrocytes, mural vascular smooth muscle cells, pericytes, and endothelial cells and regulates neurovascular coupling. A decrease in cerebral blood flow is the earliest change that occurs in AD, and is generated at the capillary level. Changes in capillary control of CBF are correlated with cognitive decline. The reduction in CBF produced by pericyte-constricting capillaries, along with subsequent decrease in CBF as a result of capillary occlusion by neutrophils and thrombi, is an important dysfunction in AD. Initial evidence indicates that reversing this reduction in CBF can restore cognitive function, provided that damage to synapses, neurons and circuits has not advanced significantly [16]. Consequently, the fNIRS screening ANN test, as described in [3], might allow early detection and therapeutic intervention to maintain CBF as a key aim for the future treatment of AD and related brain disorders.

Epidemiological studies indicate that approximately one-third of patients with AD present with vascular pathology, indicating that a strong vascular component induces diminished cerebral blood flow followed by hypoxia and a leaky blood-brain barrier [1]. Studies in the living human brain have established that aberrant cerebrovascular reactivity, CBF reduction and dysregulated CBF are prominent features of the aging–mild cognitive impairment–AD spectrum [17]. The deterioration of the brain's microvasculature, particularly in the hippocampal memory center, appears to be a very early event in the development of AD preceding the deposition of amyloid-beta (Aβ). Damaged microvasculature reduces the supply of oxygen and glucose to this region, and mitochondrial damage may additionally limit ATP production. This damage may be a function of the early increase in the expression and activity of NADPH oxidase (NOX) in endothelial cells of microvessels with age [5]. The cause of AD-related mitochondrial dysfunction is the amyloid (Aβ) cascade-induced mitochondrial dysfunction. However, other data have indicated that mitochondrial dysfunction is independent of Aβ, suggesting a primary mitochondrial cascade hypothesis. Therefore mitochondria appear to mediate Aβ production and possibly even initiate pathological molecular cascades in AD [18]. Aβ mainly disturbs the function of complexes I and IV in the respiratory chain. An increase in N1-methylation of adenosine (m1A) in ND5 mRNA might lead to dysfunction of mitochondrial complex I in an AD cell model as well as in AD patients. These findings suggest that a newly identified mechanism is likely involved in Aβ-induced mitochondrial dysfunction [19] [20]. Analyses of the associations between the activities of complexes I, II, III, and IV and citrate synthase (CS) in patients with major depressive disorder (MDD) or Alzheimer's disease (AD) and disease severity were performed for both AD and MDD patients. However, the mean values of mitochondrial parameters were significantly altered in patients with AD, but not in patients with MDD. In AD, a decrease in the activity of CS and complex IV may cause mitochondrial dysfunction, whereas an increase in the activity of other mitochondrial complexes or their ratios to CS may be an adaptive response [21].

These various NVC responses may be based not only on neuronal brain activity but also on a range of oxygen-sensing signal cascades [22] that regulate CBF, as shown in Figure 8.

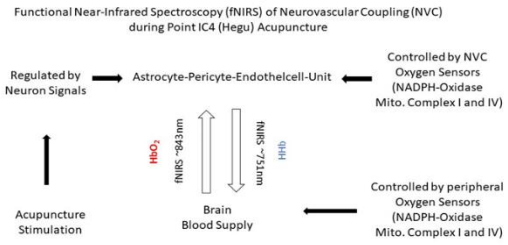

Figure 8: Shows that NVC is regulated by neuronal activity signals and controlled by oxygen sensors based on the activity of NADPH oxidase, the activity of mitochondrial complexes I and IV, and the brain blood supply controlled by peripheral oxygen sensors (NADPH oxidase, mitochondrial complexes I and IV, as described for the carotid body oxygen sensor).

Carotid body (CB) NADPH oxidase, mitochondrial complex I, and complex IV of CB type I cells are the most likely oxygen sensor candidates for initiating hypoxia-induced release of neurotransmitters (NTs) to excite synoptically connected sinus nerve fibers to regulate ventilation and blood circulation centers in the brainstem. Stimulation of NADPH oxidase by enhanced p47 binding decreases sinus nerve activity and poisoning complex I silences sinus nerve activity. Complex IV contains four redox centers, namely heme a and heme a3, which are linked by helix-X and two copper centers (CuA and CuB). Oxygen binds to the heme a3-CuB binuclear center and helix-X stretches, facilitating communication between the two heme groups and enhancing electron transfer from the mitochondrial cytochrome c (complex III) over CuA to heme a and the binuclear center. The shape of the

intracellular mitochondrial network changes by approximately 3 Å upon helix-X movement, presumably inducing a change in cell shape with variations in the activity of stretch-sensitive ion channels (Acker and Fandrey, 2022)). Under the assumption that the CB oxygen sensor mechanism might also be valid for brain NVC regulation, Figure 8 proposes that the regulatory neuron signal is controlled by oxygen sensors to optimize CBF and the brain blood supply. Assuming that NADPH oxidase is one of the oxygen sensor candidates, complexes I and IV are defective, as described for AD-linked brain disorders ([5][19] consequently brain microcirculation is dysregulated, as shown in Figure 4,7, due to a mismatch of arterial and venous perfusion. This mismatch, which results in brain hypoxia has also been observed in BDPs confronted with tasks such as calculation, smelling, tasting or music [3].

CONCLUSION

The following conclusions were drawn:

fNIRS recordings of brain Hb oxygenation indicate the efficacy of brain microcirculation and brain oxygen supply.

Central brain acupuncture stimulation revealed deficits in brain microcirculation and oxygen supply in BDPs.

A 20-second period of acupuncture stimulation results in brain hypoxia for BDPs, but not for CPs, primarily due to mismatching of arterial and venous microcirculation.

fNIRS combined with subsequent ANN analysis of the brain oxygen supply could be highly effective and user-friendly for recording early signs of brain microcirculation dysregulation and therapeutic progress.

DECLARATIONS

Acknowledgement

We thank Gisela Acker for her generous private financial support of the project and Sofia Sappia for her excellent contribution in establishing the EEG Fourier analysis.

Declaration of Interest

The authors declare that there are no conflicts of interest regarding the publication of this article.

Dr. med. Wilhelm Ehleben: head of the practice for general medicine, consultant for general medicine, physiology, emergency medicine, palliative medicine, flight medicine

Patient selection and application of fNIRS, analysis of data, and manuscript preparation

Dr. rer. nat Jörn M. Horschig: PhD, software manager, project leader

EEG power analysis, Octamon software management, manuscript preparation

Prof. (em) Dr. Med Helmut Acker: Consultant for Physiology and Acupuncture,

fNIRS data registration and analysis, needle acupuncture, manuscript preparation

REFERENCES

1. Raz L, Knoefel J, Bhaskar K. The neuropathology and cerebrovascular mechanisms of dementia. Journal of Cerebral Blood Flow and Metabolism. Nature Publishing Group; 2016. pp. 172–186. doi:10.1038/jcbfm.2015.164
2. Srinivasan S, Butters E, Collins-Jones L, Su L, O'Brien J, Bale G. Illuminating neurodegeneration: a future perspective on near-infrared spectroscopy in dementia research. Neurophotonics. 2023;10. doi:10.1117/1.nph.10.2.023514
3. Ehleben W, Horschig JM, Acker H. Artificial Neural Network Analysis of Prefrontal fnirs Blood Oxygenation Recordings Affiliation. Archives of Internal Medicine Research. 2023;6: 116–128. doi:10.26502/aimr.0156
4. Li Rihui, Nguyen Thinh, Potter Thomas, Zhang Yingchun. Dynamic cortical connectivity alterations associated with Alzheimer's disease: An EEG and fNIRS integration study. Neuroimage Clin. 2019;21: 1–11.
5. Mamelak M. The Alzheimer's Disease Brain, Its Microvasculature, and NADPH Oxidase. Journal of Alzheimer's Disease. 2023; 1–10. doi:10.3233/jad-230415
6. Andrew Ellis NWKB. GRASPING THE WIND. Brookline Massachusetts: Paradigma Publications; 1989.
7. Chavez LM, Huang SS, MacDonald I, Lin JG, Lee YC, Chen YH. Mechanisms of acupuncture therapy in ischemic stroke rehabilitation: A literature review of basic studies. International Journal of Molecular Sciences. MDPI AG; 2017. doi:10.3390/ijms18112270
8. Oldag A, Neumann J, Goertler M, Hinrichs H, Heinze HJ, Kupsch A, et al. Near-infrared spectroscopy and transcranial sonography to evaluate cerebral autoregulation in middle cerebral artery steno-occlusive disease. J Neurol. 2016;263: 2296–2301. doi:10.1007/s00415-016-8262-5
9. Davies DJ, Su Z, Clancy MT, Lucas SJE, Dehghani H, Logan A, et al. Near-Infrared Spectroscopy in the Monitoring of Adult Traumatic Brain Injury: A Review. J Neurotrauma. 2015;32: 933–941. doi:10.1089/neu.2014.3748
10. Haeussinger FB, Heinzel S, Hahn T, Schecklmann M, Ehlis AC, Fallgatter AJ. Simulation of near-infrared light absorption considering individual head and prefrontal cortex anatomy: Implications for optical neuroimaging. PLoS One. 2011;6. doi:10.1371/journal.pone.0026377
11. Scholkmann F, Tachtsidis I, Wolf M, Wolf U. Systemic physiology augmented functional near-infrared spectroscopy : a powerful approach to study the embodied human brain. Neurophotonics. 2022;9: 1–24. doi:10.1117/1.NPh.9.3.030801
12. Agbangla NF, Audiffren M, Albinet CT. Use of near-infrared spectroscopy in the investigation of brain activation during cognitive aging: A systematic review of an emerging area of research. Ageing Res Rev. 2017;38: 52–66. doi:10.1016/j.arr.2017.07.003
13. Acker H, Schmidt-Rathjens C, Acker T, Fandrey J, Ehleben W. Acupuncture–brain interactions as hypothesized by mood scale recordings. Med Hypotheses. 2015;85: 371–379. doi:10.1016/j.mehy.2015.05.013
14. Allen J. Photoplethysmography and its application in clinical physiological measurement. Physiological Measurement. Institute of Physics Publishing; 2007. pp. R1–R39. doi:10.1088/0967-3334/28/3/R01
15. Du K, Yang S, Wang J, Zhu G. Acupuncture Interventions for Alzheimer's Disease and Vascular Cognitive Disorders: A Review of Mechanisms. Oxidative Medicine and Cellular Longevity. Hindawi Limited; 2022. doi:10.1155/2022/6080282
16. Korte N, Nortley R, Attwell D. Cerebral blood flow decrease as an early pathological mechanism in Alzheimer's disease. Acta Neuropathologica. Springer Science and Business Media Deutschland GmbH; 2020. pp. 793–810. doi:10.1007/s00401-020-02215-w
17. Kisler K, Nelson AR, Montagne A, Zlokovic B V. Cerebral blood flow regulation and neurovascular dysfunction in Alzheimer disease. Nat Rev Neurosci. 2017;18: 419–434. doi:10.1038/nrn.2017.48
18. Swerdlow RH. Mitochondria and Mitochondrial Cascades in Alzheimer's Disease. Journal of Alzheimer's Disease. IOS Press; 2018. pp. 1403–1416. doi:10.3233/JAD-170585
19. Jörg M, Plehn JE, Kristen M, Lander M, Walz L, Lietz C, et al. N1-methylation of adenosine (m1A) in ND5 mRNA leads to complex I dysfunction in Alzheimer's disease. Mol Psychiatry. 2024. doi:10.1038/s41380-024-02421-y

20. Monzio Compagnoni G, Di Fonzo A, Corti S, Comi GP, Bresolin N, Masliah E. The Role of Mitochondria in Neurodegenerative Diseases: the Lesson from Alzheimer's Disease and Parkinson's Disease. Molecular Neurobiology. Springer; 2020. pp. 2959–2980. doi:10.1007/s12035-020-01926-1

21. Fišar Z, Hansíková H, Křížová J, Jirák R, Kitzlerová E, Zvěřová M, et al. Activities of mitochondrial respiratory chain complexes in platelets of patients with Alzheimer's disease and depressive disorder. Mitochondrion. 2019;48: 67–77. doi:10.1016/j.mito.2019.07.013

22. Acker T, Acker H. Cellular oxygen sensing need in CNS function: physiological and pathological implications. J Exp Biol. 2004;207: 3171–88. doi:10.1242/jeb.01075

23. Acker H, Fandrey J. Carotid body physiology meets cytochrome c oxidase crystallography Commentary to Ortega-Sáenz P, López-Barneo J. Physiology of the Carotid Body: From Molecules to Disease. Annu Rev Physiol 82: 127–149, 2020. Torres-Torrelo H, Ortega-Sáenz P, Gao L, López-. Pflugers Arch. 2022;474: 187–189. doi:10.1007/s00424-021-02662-8